THE JOURNAL OF PHYSICAL CHEMISTRY C

Article

pubs.acs.org/JPCC

Improved Hydrogen Storage Performance of MgH_2−$LiAlH_4$ Composite by Addition of $MnFe_2O_4$

Qi Wan,[†] Ping Li,[*,†] Ziliang Li,[†] Fuqiang Zhai,[‡] Xuanhui Qu,[†,§] and Alex A. Volinsky[∥]

[†]Institute for Advanced Materials and Technology, University of Science and Technology Beijing, Beijing 100083, China

[‡]Departament Física Aplicada, EETAC, Universitat Politècnica de Catalunya-BarcelonaTech, 08860 Castelldefels, Spain

[§]State Key Laboratory for Advanced Metals and Materials, University of Science and Technology Beijing, Beijing 100083, China

[∥]Department of Mechanical Engineering, University of South Florida, Tampa, Florida 33620, United States

Supporting Information

ABSTRACT: The catalytic effects of $MnFe_2O_4$ nanoparticles on the hydrogen storage properties of MgH_2−$LiAlH_4$, prepared by ball milling, are studied for the first time. The hydrogen storage properties and reaction mechanism are investigated by pressure−composition−temperature (PCT), differential scanning calorimetry (DSC), X-ray diffraction (XRD), and X-ray photoelectron spectroscopy (XPS). The nonisothermal desorption results show that MgH_2−$LiAlH_4$ + 5 mol % $MnFe_2O_4$ has a lower onset dehydrogenation temperature, 85, 50, and 40 °C lower than these of ball-milled MgH_2−$LiAlH_4$ sample for each stage in the dehydrogenation process. The isothermal dehydriding kinetics and isothermal rehydrogenation kinetics results indicate that adding $MnFe_2O_4$ to MgH_2−$LiAlH_4$ could significantly enhance the absorption/desorption kinetics of MgH_2−$LiAlH_4$. From the differential scanning calorimetry and Kissinger analysis, the apparent activation energy of the 5 mol % $MnFe_2O_4$-doped sample for the three decomposition stage is 55.8, 70.8, and 96.5 kJ/mol, resulting in a 45.7, 85.5, and 99.6 kJ/mol decrease, respectively, compared with the MgH_2−$LiAlH_4$ sample. These improvements are mainly attributed to in situ formed $Fe_{0.872}O$ phase and the amorphous Mn-containing phase during the dehydrogenation process, which act as the real catalyst in the MgH_2−$LiAlH_4$ + 5 mol % $MnFe_2O_4$ composite.

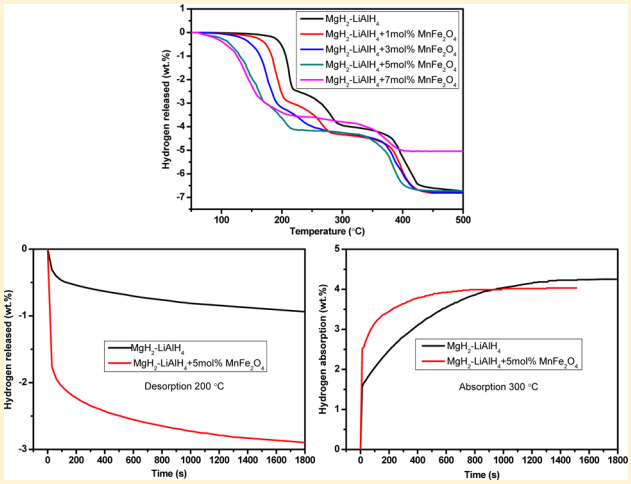

1. INTRODUCTION

Large gravimetric (≥5.5 wt %) and volumetric (≥40 g/L) densities are extremely eager for on-board hydrogen storage in fuel cell vehicles according to the U.S. DOE's 2015 target.[1] Magnesium hydride having high theoretical hydrogen storage capacity (7.6 wt %), abundant resources, and low cost can fully satisfy the demand of application.[2−6] However, high desorption temperature (>400 °C) and relatively poor hydriding−dehydriding kinetics limit magnesium hydride practical applications.[5−8] During the past decade researchers tried to address these challenges. Efforts included preparing nanoparticles by high-energy ball milling[9] and adding catalysts, such as metals,[5,9,10] C-containing species,[11−14] metal oxides,[15−18] metal halides,[19,20] and other compounds.[21−23] However, these endeavors could only strengthen its absorption/desorption kinetics properties. Thermodynamic performances of the magnesium hydride could hardly be changed.[24] From this view, researchers tried to destabilize MgH_2 using complex hydride with a high gravimetric density such as $LiAlH_4$, which is an effective way to improve the hydrogen storage properties of MgH_2 and $LiAlH_4$.[24−29] However, the hydrogen storage performances of the MgH_2−$LiAlH_4$ still need further improvement for practical application as a suitable hydrogen storage material, and the reaction mechanism and thermodynamics also require being demonstrated in more detail. Li et al.[30] and Zhai et al.[31] reported that $MnFe_2O_4$ nanoparticles could remarkably improve the dehydrogenation properties of MgH_2 and $LiAlH_4$ alone. Therefore, it is reasonable to assume that $MnFe_2O_4$ would show great potential as a catalyst to promote MgH_2−$LiAlH_4$ system hydrogen storage performances. Motivated by the above findings, in this study, $MnFe_2O_4$ nanoparticles are employed as catalyst to study their effect on the hydrogen storage properties of the MgH_2−$LiAlH_4$ system by high-energy ball milling.

2. EXPERIMENTAL SECTION

Pure $LiAlH_4$ (hydrogen storage grade, ≥93% purity) and MgH_2 (hydrogen storage grade) were purchased from Sigma Aldrich

Received: October 22, 2013
Revised: December 1, 2013
Published: December 4, 2013

Co., and $MnFe_2O_4$ (≥99.99% purity, 20 nm particle size) was prepared by nitrate−citrate autocombustion methods. Details of the preparation procedure are given in our previous reports.[30,32] All materials were used directly, with no further purification. All handling (including weighing and loading) was conducted in a glovebox filled with high-purity argon (99.999%) in order to prevent oxidation and moisture. Approximately 3 g of MgH_2−$LiAlH_4$ was mixed with different mole fractions (1, 3, 5, and 7 mol %) of $MnFe_2O_4$ nanoparticles and then ball milled for 30 min in a high-energy Spex Mill. MgH_2 and $LiAlH_4$ with a molar ratio of 1:1 will be referred to as MgH_2−$LiAlH_4$ for simplicity. MgH_2−$LiAlH_4$ was also prepared under the same conditions for comparison purposes. All samples were loaded into a 80 mL stainless steel pot in an argon-filled glovebox. ZrO_2 balls were added with a ball-to-powder weight ratio of 15:1. Samples were first ball milled for 10 min and then cooled down for 5 min after each cycle.

Hydrogen absorption and desorption properties of undoped and doped MgH_2−$LiAlH_4$ samples were measured using a pressure−composition−temperature (PCT) apparatus (Beijing Nonferrous Metal Research Institute, China). The highest pressure and temperature of the apparatus can be operated up to 10 MPa and 600 °C. The pressure of hydrogen in relation to volume was displayed by a pressure transducer. Experimental studies were done by a reactor that consisted of two parts: a heater and sample vessel. The former was used to connect with the pressure transducer and thermocouple. The reactor had a 1.5 cm outer diameter (o.d.), 0.5 cm wall, and 20 cm internal length, and it was loaded with the sample vessel (1 cm o.d., 0.1 cm wall, and 5 cm internal length). The reactor was heated with an air furnace. The mass of the sample used for measuring was kept at 0.3 g for each time, and the error range of temperature was controlled within ±1 °C. From the value of hydrogen pressure change, the amount of hydrogen absorbed and desorbed could be obtained.[33,34] For nonisothermal dehydrogenation, 0.5 g of the sample was loaded into the sample vessel in the glovebox and then heated up to 500 °C at a heating rate of 4 °C/min under 0.1 MPa atm pressure. The isothermal dehydrogenation behavior for undoped and doped samples was carried out at 200 and 300 °C under 0.1 MPa pressure, respectively. Following the first complete dehydrogenation, samples were subjected to rehydrogenation studies at 300 °C under 3 MPa of hydrogen pressure. The dehydrogenation/rehydrogenation amounts, calculated for all samples, were converted to pure MgH_2−$LiAlH_4$ with elimination of various impurities.

For analyzing the dehydrogenation performance and calculating the desorption activation energy of the undoped and doped MgH_2−$LiAlH_4$ sample by means of the Kissinger method, differential scanning calorimetry (DSC) was performed using NETZSCH STA 449C under a high-purity argon (99.999%) flow rate of 50 mL/min. About 5 mg of the sample was sealed into a 50 mL alumina crucible in the glovebox and then heated at different rates (4, 7, and 10 °C/min) from 50 to 500 °C.

Microstructural characterization of the samples after ball milling, after dehydrogenation, and after rehydrogenation was determined using the MXP21VAHF X-ray diffractometer with Cu Kα radiation (40 kV, 200 mA) at room temperature. The 2θ angle was varied from 10° to 90° in 0.02° increments. X-ray photoelectron spectroscopy (XPS) was performed with the PHI-5300 spectrometer.

3. RESULTS AND DISCUSSION

Figure 1 presents the nonisothermal desorption curves of ball-milled MgH_2−$LiAlH_4$ and ball-milled MgH_2−$LiAlH_4$ doped with 1, 3, 5, and 7 mol % $MnFe_2O_4$ nanoparticles. Desorption curves distinctly reveal that doping $MnFe_2O_4$ nanoparticles notably ameliorates MgH_2−$LiAlH_4$ dehydrogenation properties, resulting in a remarkable reduction of the desorption temperature. For the ball-milled MgH_2−$LiAlH_4$ sample, three significant dehydrogenation stages are observed during the whole heating process: the first stage and second stage within the temperature ranges from 140 to 220 and 220 to 300 °C appear to be the first and second decomposition of $LiAlH_4$. The third stage within the temperature ranging from 340 to 430 °C corresponds to the MgH_2-relevant decomposition, agreeing well with previous literature,[35] and a total hydrogen release capacity of 6.71 wt % is obtained during these three decomposition processes.

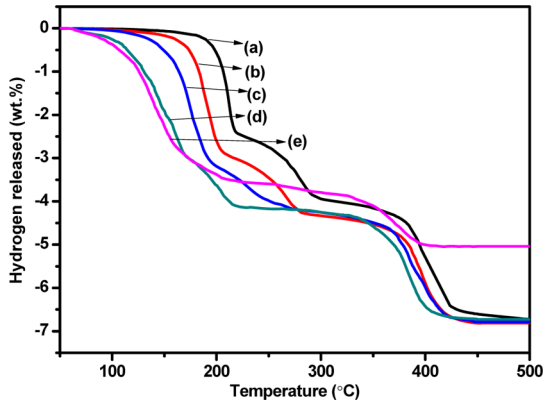

Figure 1. Thermal desorption curves of (a) ball-milled MgH_2−$LiAlH_4$ and ball-milled MgH_2−$LiAlH_4$ doped with (b) 1, (c) 3, (d) 5, and (e) 7 mol % $MnFe_2O_4$.

While for the $MnFe_2O_4$-doped samples, three stages of dehydrogenation are observed during the heating process. For the 1 mol % doped sample, the dehydrogenation process starts at 110 °C and terminates at 205 °C for the first decomposition stage and initiates at 205 and 325 °C and ends at 280 and 415 °C for the second and third decomposition steps, respectively. Further increase of additives amounts to 3 mol %; the onset dehydrogenation temperature reduces to 90, 195, and 310 °C for the three stages. Compared with ball-milled MgH_2−$LiAlH_4$, adding 1 and 3 mol % of $MnFe_2O_4$ causes a reduction in the onset desorption temperature of 30 and 50 °C for the first step, 15 and 25 °C for the second step, and 15 and 30 °C for the third step, respectively. During the three dehydrogenation processes, the sample with 1 mol % $MnFe_2O_4$ releases about 6.82 wt % hydrogen for three stages whereas 6.78 wt % hydrogen is desorbed for the 3 mol % doped sample, while for the ball-milled MgH_2−$LiAlH_4$ + 5 mol % $MnFe_2O_4$ sample three stages of dehydrogenation occur during the heating process with a total hydrogen release amount of 6.74 wt %. The first stage proceeds in the temperature ranging from 55 to 170 °C, which is 85 and 50 °C lower than those of ball-milled MgH_2−$LiAlH_4$. The second stage takes place from 170 to 210 °C, resulting in 50 and 90 °C decreases, respectively. The third stage starts at 300 °C and is completed at 400 °C, causing reduction of 40 and 30 °C. With the amount of additive increasing to 7 mol %, the onset dehydrogenation temperature

decreases to 53, 160, and 270 °C, respectively, which indicates $MnFe_2O_4$ nanoparticles can significantly improve the dehydrogenation performance of the MgH_2−$LiAlH_4$ system. However, the desorption hydrogen content for the 7 mol % doped sample is only 5.04 wt % for the three steps, signifying a severe reduction in the hydrogen desorption capacity due to an excessive amount of $MnFe_2O_4$ nanoparticles. Therefore, the 5 mol % $MnFe_2O_4$ doped MgH_2−$LiAlH_4$ sample exhibits optimal dehydriding property, including the desorption temperature and hydrogen released capacity. Thus, utilizing the optimal 5 mol % $MnFe_2O_4$-doped sample allows analyzing the $MnFe_2O_4$ catalytic mechanism in the following tests.

The dehydrogenation behavior of ball-milled MgH_2−$LiAlH_4$ and ball-milled MgH_2−$LiAlH_4$ doped with 5 mol % $MnFe_2O_4$ sample is further studied by DSC. Figure 2 shows the DSC curves of ball-milled MgH_2−$LiAlH_4$ sample and ball-milled MgH_2−$LiAlH_4$ doped with 5 mol % $MnFe_2O_4$ sample within 50−500 °C at a heating rate of 10 °C/min. As shown in Figure 2a, the DSC curve of the ball-milled MgH_2−$LiAlH_4$ sample includes five distinct characteristics peaks, corresponding to two exothermic processes and three endothermic processes. The first exothermic peak turns up at 142.4 °C, corresponding to the interaction of $LiAlH_4$ with surface hydroxyl impurities,[31,36−39] and the first endothermic peak appears at 168.1 °C arising from melting of $LiAlH_4$.[40−42] The second exothermic peak occurs at 180.7 °C due to decomposition of $LiAlH_4$ to Li_3AlH_6. The second and third endothermic peaks at 225.1 and 349.0 °C are both attributed to the MgH_2-relevant decomposition.[35] Compared with the DSC plot of ball-milled MgH_2−$LiAlH_4$ sample, the thermal decomposition behavior of MgH_2−$LiAlH_4$ + 5 mol % $MnFe_2O_4$ sample is markedly different, showing one exothermic peak and two broad endothermic peaks, in good agreement with reports.[35,43] The exothermic peak occurs at 105.6 °C, and the first endothermic peak appears at 142.1 °C, which is attributed to decomposition of $LiAlH_4$ to Li_3AlH_6 and H_2 and decomposition of Li_3AlH_6 to LiH, Al, and H_2, which is comparable with the three dehydrogenation steps in Figure 1 and in accord with literature,[35] but at a much lower temperature than the ball-milled MgH_2−$LiAlH_4$ sample. Results demonstrate that $LiAlH_4$ starts to decompose at a little lower temperature before melting after adding $MnFe_2O_4$ catalyst, which agrees well with the results of ball-milled $LiAlH_4$ doped with 7 mol % $MnFe_2O_4$ reported by Zhai et al.[31] The second endothermic peak at 324.6 °C corresponds to the MgH_2-relevant decomposition, which is analogous to that of the MgH_2−$LiAlH_4$ sample. The remarkable decrease of the value of peak temperature in DSC curves indicates the dehydriding performances of ball-milled MgH_2−$LiAlH_4$ are improved by $MnFe_2O_4$ nanoparticles. Nevertheless, the broad peak in the DSC curve of the MgH_2−$LiAlH_4$ + 5 mol % $MnFe_2O_4$ sample indicates a faster desorption kinetics performance at lower temperature. In addition, the decomposition temperature measured by DSC is higher than that tested by PCT. A similar phenomenon is also observed in the literature.[35,38,39] These differences may result from the fact that the desorption measurement is carried out under different conditions for the samples tested with DSC (0.1 MPa argon, 10 °C/min) and PCT (0.1 MPa atm, 4 °C/min), resulting in different driving forces during the dehydrogenation process.

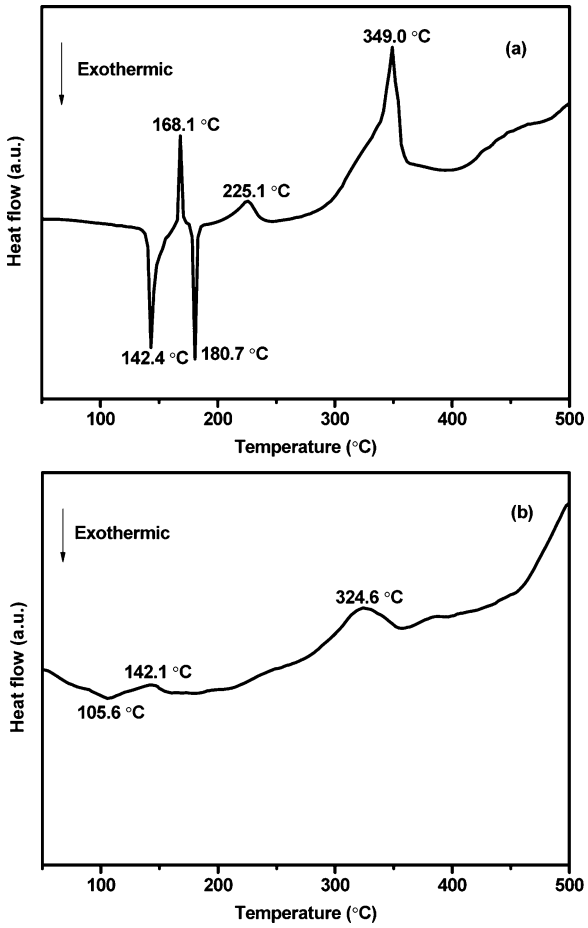

Figure 2. DSC profiles of (a) ball-milled MgH_2−$LiAlH_4$ and (b) ball-milled MgH_2−$LiAlH_4$ doped with 5 mol % $MnFe_2O_4$ within the 50−500 °C temperature range (10 °C/min heating rate).

In order to analyze the mechanism in the dehydrogenation process, X-ray diffraction is performed on ball-milled MgH_2−$LiAlH_4$ doped with 5 mol % $MnFe_2O_4$. Figure 3 shows the XRD patterns of the ball-milled MgH_2−$LiAlH_4$ doped with 5 mol % $MnFe_2O_4$ after ball milling and after dehydrogenation at different temperatures. For the ball-milled sample, MgH_2 and $LiAlH_4$ phases are observed; a minor $MnFe_2O_4$ phase is detected. After the sample heats to 200 °C, $LiAlH_4$ phase disappears, new phases LiH and Al appear, while the MgH_2 phase still exists. Moreover, a small amount of $Li_{0.92}Mg_{4.08}$ phase and $Fe_{0.872}O$ phases are observed, indicating that hydrogen desorption from the doped sample below 200 °C is mainly attributed to dehydrogenation of $LiAlH_4$ with a small amount of MgH_2-relevant decomposition. After heating to 300 °C, peaks of the MgH_2 and LiH/Al phases become weaker and a new $Al_{12}Mg_{17}$ phase is formed. Meanwhile, the amount of $Li_{0.92}Mg_{4.08}$ phase increases, and the $Fe_{0.872}O$ phase still exists. On further heating to 400 °C, the intensity of $Li_{0.92}Mg_{4.08}$ and $Al_{12}Mg_{17}$ phases becomes stronger, the peaks of MgH_2, LiH, and Al phases disappear, and the $Fe_{0.872}O$ phase still can be observed, indicating that the hydrogen desorption in the temperature range of 200−400 °C is mainly due to reactions of Al and LiH with MgH_2. According to the above results, the following reactions may take place during MgH_2-relevant decomposition in the temperature range of 200−400 °C

$$4.08MgH_2 + 0.92LiH \rightarrow Li_{0.92}Mg_{4.08} + 4.54H_2 \quad (1)$$

$$17MgH_2 + 12Al \rightarrow Al_{12}Mg_{17} + 17H_2 \quad (2)$$

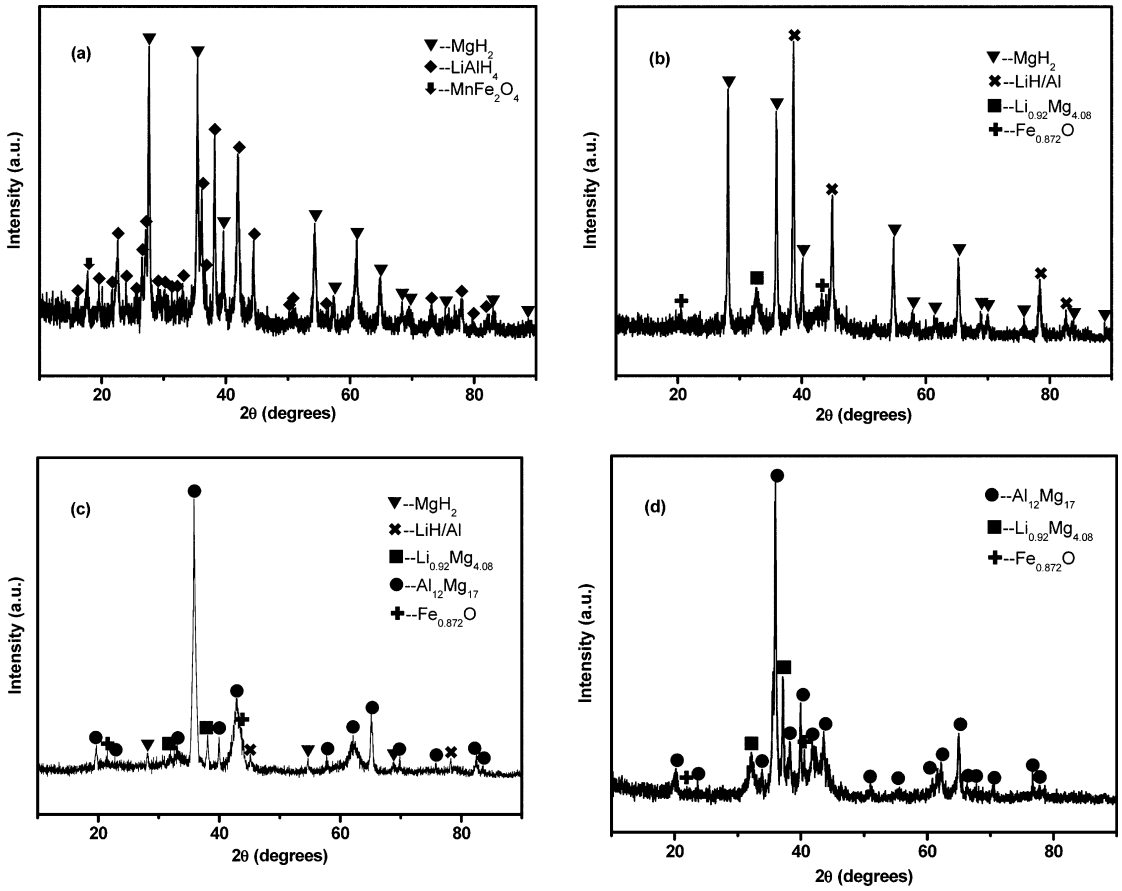

Figure 3. XRD patterns of the MgH_2−$LiAlH_4$ + 5 mol % $MnFe_2O_4$ composite (a) after ball milling and after dehydrogenation at (b) 200, (c) 300, and (d) 400 °C.

Al−Mg and Li−Mg alloys are observed in this paper, which is accord with other literature.[24,25,27,43] In addition, a new phase $Fe_{0.872}O$ is detected for the doped samples after decomposition at different temperatures, indicating that a reaction between $LiAlH_4$ and the $MnFe_2O_4$ catalyst happened during the dehydriding process. Nevertheless, no diffraction peaks of Mn-containing phase are observed due to the relatively lower amount or being in an amorphous phase.[31,37,39]

The outstanding catalytic effect of $MnFe_2O_4$ nanoparticles on accelerating the dehydrogenation kinetics property of ball-milled MgH_2−$LiAlH_4$ sample is further demonstrated by examination of isothermal desorption at constant temperature. For comparison, the desorption kinetics performance of ball-milled MgH_2−$LiAlH_4$ sample is examined under the same conditions. Figures 4 and 5 show the dehydrogenation kinetics curves of ball-milled MgH_2−$LiAlH_4$ and MgH_2−$LiAlH_4$ + 5 mol % $MnFe_2O_4$ samples at 200 and 300 °C under 0.1 MPa, respectively. It can be seen from Figure 4 that the ball-milled MgH_2−$LiAlH_4$ system and the MgH_2−$LiAlH_4$ + 5 mol % $MnFe_2O_4$ sample release 0.94 and 2.91 wt % hydrogen at 200 °C in 1800 s under 0.1 MPa pressure, respectively. Further increasing the temperature to 300 °C, the MgH_2−$LiAlH_4$ + 5 mol % $MnFe_2O_4$ sample desorbs 4.09 wt % hydrogen within 15 s, which is much higher than that of MgH_2−$LiAlH_4$ sample (0.31 wt %) and TiF_3-doped sample reported by Mao et al.[35] In contrast, about 1800 s is required for the ball-milled MgH_2−$LiAlH_4$ sample to release 4.08 wt % hydrogen under the same conditions, which demonstrates $MnFe_2O_4$ superiority in improving MgH_2−$LiAlH_4$ dehydrogenation kinetics properties.

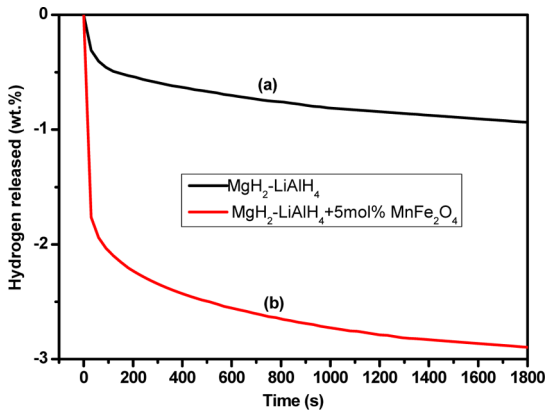

Figure 4. Isothermal desorption curves of (a) MgH_2−$LiAlH_4$ and (b) MgH_2−$LiAlH_4$ + 5 mol % $MnFe_2O_4$ samples at 200 °C.

Therefore, significant improvement of MgH_2−$LiAlH_4$ desorption kinetics can be obtained by adding $MnFe_2O_4$ nanopowders.

The desorption kinetics enhancement is connected with the energy barriers for hydrogen desorption. For investigating the dehydrogenation kinetics enhancement of the MgH_2−$LiAlH_4$ + 5 mol % $MnFe_2O_4$ sample in detail, DSC curves at different heating rates are measured to calculate the apparent activation energies of undoped and doped MgH_2−$LiAlH_4$ samples by the Kissinger method according to the following equation[44]

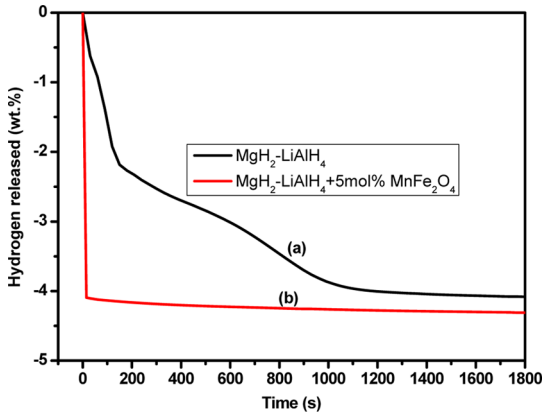

Figure 5. Isothermal desorption curves of (a) MgH_2−$LiAlH_4$ and (b) MgH_2−$LiAlH_4$ + 5 mol % $MnFe_2O_4$ samples at 300 °C.

$$\frac{d\ \ln(\beta/T_p^{\ 2})}{d(1/T_p)} = -\frac{E_a}{R} \tag{3}$$

where β is the heating rate, R is the gas constant, and T_p is the value of the peak temperature in the DSC curve. Therefore, the apparent activation energy, E_a, can be obtained from the slope in a plot of $\ln(\beta/T_p^{\ 2})$ versus $1000/T_p$. The apparent activation energy of ball-milled MgH_2−$LiAlH_4$ sample is calculated to be 101.5, 156.3, and 196.1 kJ/mol, while these values decrease to 55.8, 70.8, and 96.5 kJ/mol for 5 mol % $MnFe_2O_4$-doped MgH_2−$LiAlH_4$ sample. These results provide quantitative evidence for reduced desorption kinetics barriers during the dehydriding process, which indicates that $MnFe_2O_4$ nanoparticles can significantly improve the dehydrogenation performance of the ball-milled MgH_2−$LiAlH_4$ system.

In order to investigate the reversibility of the ball-milled MgH_2−$LiAlH_4$ and ball-milled MgH_2−$LiAlH_4$ doped with 5 mol % $MnFe_2O_4$ sample, rehydrogenation of the dehydrogenated sample is performed at 300 °C under 3 MPa of hydrogen pressure. Figure 6 presents the rehydrogenation kinetics curves of the ball-milled MgH_2−$LiAlH_4$ sample and MgH_2−$LiAlH_4$ + 5 mol % $MnFe_2O_4$ sample at 300 °C under 3 MPa hydrogen pressure. It can be evidently seen from Figure 6 that the MgH_2−$LiAlH_4$ + 5 mol % $MnFe_2O_4$ sample shows better rehydrogenation kinetics property than the MgH_2−$LiAlH_4$ sample. For the ball-milled MgH_2−$LiAlH_4$ sample, 2.81 wt % hydrogen is absorbed within 300 s. However, a hydrogen absorption capacity of 3.64 wt % is reached within 300 s for the MgH_2−$LiAlH_4$ + 5 mol % $MnFe_2O_4$ sample, which is higher than that of MgH_2−$LiAlH_4$ sample and TiF_3-doped sample in other report.[35] These results demonstrate that the $MnFe_2O_4$ nanoparticles catalyst also remarkably improves the rehydrogenation kinetics performance of the MgH_2−$LiAlH_4$ sample.

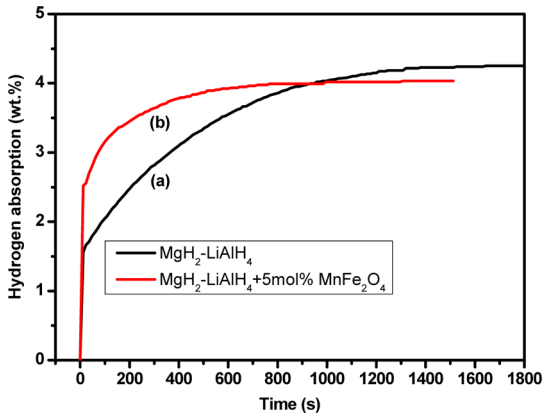

Figure 6. Isothermal rehydrogenation kinetics of (a) MgH_2−$LiAlH_4$ and (b) MgH_2−$LiAlH_4$ + 5 mol % $MnFe_2O_4$ samples at 300 °C under 3 MPa.

To determine the rehydrogenation product, XRD analysis is carried out on the ball-milled MgH_2−$LiAlH_4$ sample and MgH_2−$LiAlH_4$ + 5 mol % $MnFe_2O_4$ sample after rehydrogenation at 300 °C under 3 MPa hydrogen pressure, as presented in Figure 7. It is distinct that phases MgH_2, LiH, and Al (Al and LiH peaks overlapping in the XRD patterns) are observed in both the undoped and the doped MgH_2−$LiAlH_4$ samples. However, no $Al_{12}Mg_{17}$ or $Li_{0.92}Mg_{4.08}$ alloy is detected in the rehydrogenated samples, indicating that full recovery of LiH and MgH_2 from $Li_{0.92}Mg_{4.08}$ and $Al_{12}Mg_{17}$ alloys has been achieved, as reported in the literature[24,25,43] as follows

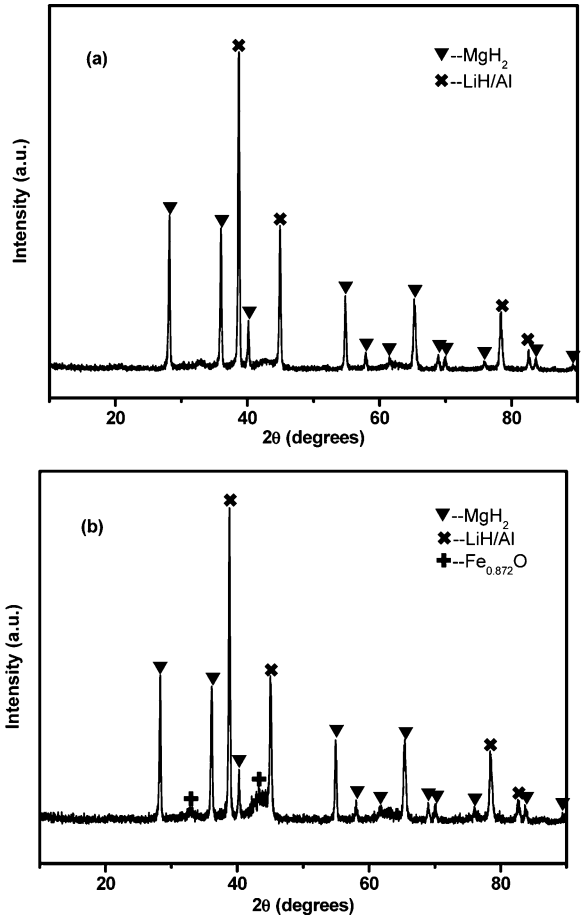

Figure 7. XRD patterns of (a) MgH_2−$LiAlH_4$ and (b) MgH_2−$LiAlH_4$ + 5 mol % $MnFe_2O_4$ samples after rehydrogenation at 300 °C under 3 MPa.

$$Al_{12}Mg_{17} + 17H_2 \rightarrow 17MgH_2 + 12Al \tag{4}$$

$$Li_{0.92}Mg_{4.08} + 4.5H_2 \rightarrow 4.08MgH_2 + 0.92LiH \tag{5}$$

In addition, $Fe_{0.872}O$ phase is present in the rehydrogenated MgH_2−$LiAlH_4$ + 5 mol % $MnFe_2O_4$ sample, which is also detected in the dehydrogenated MgH_2−$LiAlH_4$ + 5 mol % $MnFe_2O_4$ sample. The formed $Fe_{0.872}O$ phase may be attributed

to reaction between $LiAlH_4$ and $MnFe_2O_4$ during the heating process, demonstrating that the $MnFe_2O_4$ nanoparticles in the ball-milled MgH_2−$LiAlH_4$ doped with 5 mol % $MnFe_2O_4$ sample have a catalytic effect through formation of $Fe_{0.872}O$ phase and Mn-containing catalytic phase. Nevertheless, no phase containing Mn is observed after ball milling, after dehydrogenation, or after rehydrogenation due to the relatively lower amount or being in an amorphous phase. A study has been reported on the catalytic effect of $MnFe_2O_4$ on decomposition of $LiAlH_4$, where the formed Fe oxide and the amorphous Mn-containing phase[31] have a catalytic effect, which leads to improved hydrogen storage performances. The catalytic effect of Fe oxide and the Mn-containing species has also been proved to be important in improving the hydrogen storage properties of MgH_2.[30] The dehydrogenation/hydrogenation properties are closely related with particle sizes and surface defects. The higher refinement is induced by adding $MnFe_2O_4$ nanoparticles. The refined particle size renders much shorter diffusion paths for hydrogen in the dehydrogenation/hydrogenation process. A decrease in particle size and crystallite size results in introducing a high surface defect density and creating more grain boundaries, which leads to surface activation and a larger surface area of MgH_2 and $LiAlH_4$ particles. Deformed and disordered surface regions are produced around finely dispersive Fe oxide and the Mn-containing species, exhibiting a lot of surface defects, which introduce a larger amount of reaction nucleation sites and hydrogen diffusion channels at the surface of the matrix for the dehydrogenation/hydrogenation process. The higher surface defect density and grain boundaries introduced by the dispersive Fe oxide and Mn-containing species improve the hydrogen storage properties. On the basis of the results reported above and the experimental results it can be concluded that the $MnFe_2O_4$ nanoparticles in the ball-milled MgH_2−$LiAlH_4$ doped with 5 mol % $MnFe_2O_4$ sample play a catalytic effect through formation of $Fe_{0.872}O$ and the amorphous Mn-containing catalytic species, which may accelerate interaction of MgH_2 and $LiAlH_4$ and thus promote the hydrogen storage properties of the MgH_2−$LiAlH_4$ sample.

To further analyze the nature of the Mn and Fe species after the ball milling, dehydrogenation, and rehydrogenation process, chemical characterization of Fe and Mn has been investigated by XPS in ball-milled, dehydrogenation, and rehydrogenation MgH_2−$LiAlH_4$ + 5 mol % $MnFe_2O_4$ samples. Figure 8 shows the XPS narrow scan spectra of Fe 2p for ball-milled, dehydrogenation, and rehydrogenation samples. The photoemission spectra of Fe 2p for ball-milled, dehydrogenation, and rehydrogenation samples all lie at 707.00 eV, corresponding to $Fe_{0.872}O_2$.[30] Figure 9 shows the XPS narrow scan spectra of Mn 2p for ball-milled, dehydrogenation, and rehydrogenation samples. The photoemission spectra of Mn 2p for ball-milled, dehydrogenation, and rehydrogenation samples all are located at 652.9 eV, corresponding to MnO_x/Mn_2.[30] XPS results further demonstrate that $MnFe_2O_4$ can notably improve the dehydrogenation/rehydrogenation hydrogen properties of the MgH_2−$LiAlH_4$ system by formation of $Fe_{0.872}O$ and the amorphous Mn-containing catalytic species.

4. CONCLUSION

The hydrogen storage properties of MgH_2−$LiAlH_4$ are effectively improved by adding $MnFe_2O_4$ nanoparticles. Non-isothermal desorption measurement results show that the onset desorption temperature of the ball-milled MgH_2−$LiAlH_4$-doped with 5 mol % $MnFe_2O_4$ is 55, 170, and 300 °C for the three steps, releasing 6.74 wt % hydrogen, resulting in a 85, 50, and 40 °C decrease, respectively, compared with the ball-milled MgH_2−$LiAlH_4$ sample. Isothermal dehydriding kinetics shows that the ball-milled MgH_2−$LiAlH_4$ system and MgH_2−$LiAlH_4$ + 5 mol % $MnFe_2O_4$ sample release 0.94 and 2.91 wt % hydrogen at 200 °C in 1800 s under 0.1 MPa pressure, respectively. On further increasing the temperature to 300 °C, the MgH_2−$LiAlH_4$ + 5 mol % $MnFe_2O_4$ sample releases 4.09 wt % hydrogen within 15 s while the ball-milled MgH_2−$LiAlH_4$ sample only releases 0.31 wt % hydrogen under the same conditions, which demonstrates the $MnFe_2O_4$ nanoparticles can remarkably improve the dehydrogenation kinetics of MgH_2−$LiAlH_4$. Rehydrogenation kinetics measurement results show that 2.81 wt % hydrogen is absorbed at 300 °C within 300 s under a hydrogen pressure of 3 MPa for the ball-milled MgH_2−$LiAlH_4$ sample. However, a hydrogen absorption capacity of 3.64 wt % is reached under the same conditions for the MgH_2−$LiAlH_4$ + 5 mol % $MnFe_2O_4$ composite, which indicates the $MnFe_2O_4$ nanoparticles also remarkably improve the rehydrogenation kinetics performance of MgH_2−$LiAlH_4$. From differential scanning calorimetry and Kissinger analysis, the apparent activation energy of the 5 mol % $MnFe_2O_4$-doped

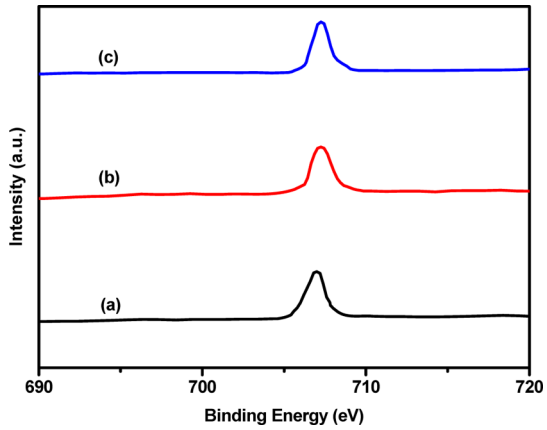

Figure 8. Narrow scan Fe 2p XPS of MgH_2−$LiAlH_4$ + 5 mol % $MnFe_2O_4$ (a) after ball milling, (b) after complete dehydrogenation, and (c) after rehydrogenation.

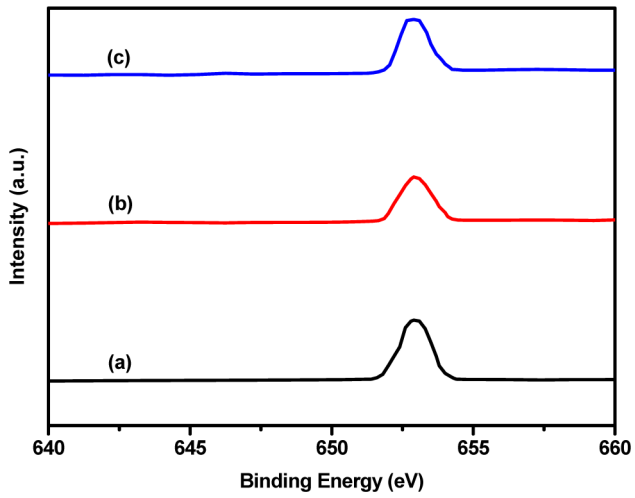

Figure 9. Narrow scan Mn 2p XPS of MgH_2−$LiAlH_4$ + 5 mol % $MnFe_2O_4$ (a) after ball milling, (b) after complete dehydrogenation, and (c) after rehydrogenation.

sample for the three decomposition stages is 55.8, 70.8, and 96.5 kJ/mol, resulting in a 45.7, 85.5, and 99.6 kJ/mol reduction, respectively, compared with the ball-milled MgH_2−$LiAlH_4$ sample. The high catalytic activity of $MnFe_2O_4$ is associated with in situ formation of the Fe oxide phase and the amorphous Mn-containing phase from $MnFe_2O_4$ and $LiAlH_4$ during the dehydrogenation process. Therefore, the formed $Fe_{0.872}O$ phase and the amorphous Mn-containing phase act as real catalysts, which ameliorates the hydrogen storage properties of the MgH_2−$LiAlH_4$ + 5 mol % $MnFe_2O_4$ composite.

■ ASSOCIATED CONTENT

Supporting Information

DSC curves of as-milled MgH_2−$LiAlH_4$ and MgH_2−$LiAlH_4$ + 5 mol % $MnFe_2O_4$ at heating rates of 4, 7, and 10 °C/min. This material is available free of charge via the Internet at http://pubs.acs.org.

■ AUTHOR INFORMATION

Corresponding Author

*Phone: +86-10-82377286. Fax: +86-10-62334311. E-mail: ustbliping@126.com.

Notes

The authors declare no competing financial interest.

■ ACKNOWLEDGMENTS

The authors acknowledge financial support from the National High-Tech R&D Program (863 Program) of China (2006AA05Z132). F. Q. Zhai thanks the China Scholarship Council (CSC) for providing the scholarship.

■ REFERENCES

(1) Yang, J.; Sudik, A.; Wolverton, C.; Siegel, D. J. High Capacity Hydrogen Storage Materials: Attributes for Automotive Applications and Techniques for Materials Discovery. *Chem. Soc. Rev.* **2010**, *39*, 656−675.

(2) Jain, I. P. Hydrogen the Fuel for 21st Century. *Int. J. Hydrogen Energy* **2009**, *34*, 7368−7378.

(3) Jain, I. P.; Lal, C.; Jain, A. Hydrogen Storage in Mg: A Most Promising Material. *Int. J. Hydrogen Energy* **2010**, *35*, 5133−5144.

(4) Song, M. Y.; Kwak, Y. J.; Lee, S. H.; Song, J. Y.; Mumm, D. R. Enhancement of Hydrogen-Storage Performance of MgH_2 by Mg_2Ni Formation and Hydride-Forming Ti Addition. *Int. J. Hydrogen Energy* **2012**, *37*, 18133−18139.

(5) Gasan, H.; Celik, O. N.; Aydinbeyli, N.; Yaman, Y. M. Effect of V, Nb, Ti and Graphite Additions on the Hydrogen Desorption Temperature of Magnesium Hydride. *Int. J. Hydrogen Energy* **2012**, *37*, 1912−1918.

(6) Pighin, S. A.; Capurso, G.; Russo, S. L.; Peretti, H. A. Hydrogen Sorption Kinetics of Magnesium Hydride Enhanced by the Addition of Zr_8Ni_{21} Alloy. *J. Alloys Compd.* **2012**, *530*, 111−115.

(7) Pitt, M. P.; Paskevicius, M.; Webb, C. J.; Sheppard, D. A.; Buckley, C. E.; Gray, E. M. The Synthesis of Nanoscopic Ti Based Alloys and Their Effects on the MgH_2 System Compared with the MgH_2+0.01Nb_2O_5 Benchmark. *Int. J. Hydrogen Energy* **2012**, *37*, 4227−4237.

(8) Baricco, M.; Rahman, M. W.; Livraghi, S.; Castellero, A.; Enzo, S.; Giamello, E. Effects of $BaRuO_3$ Addition on Hydrogen Desorption in MgH_2. *J. Alloys Compd.* **2012**, *536*, S216−S221.

(9) Xie, L.; Liu, Y.; Zhang, X. Z.; Qu, J. L.; Wang, Y. T.; Li, X. G. Catalytic Effect of Ni Nanoparticles on the Desorption Kinetics of MgH_2 Nanoparticles. *J. Alloys Compd.* **2009**, *482*, 388−392.

(10) Tanniru, M.; Slattery, D. K.; Ebrahimi, F. A Study of Stability of MgH_2 in Mg-8 atom %Al Alloy Powder. *Int. J. Hydrogen Energy* **2010**, *35*, 3555−3564.

(11) Konarova, M.; Tanksale, A.; Beltramini, J. N.; Lu, G. Q. Porous MgH_2/C Composite with Fast Hydrogen Storage Kinetics. *Int. J. Hydrogen Energy* **2012**, *37*, 8370−8378.

(12) Ranjbar, A.; Ismail, M.; Guo, Z. P.; Yu, X. B.; Liu, H. K. Effects of CNTs on the Hydrogen Storage Properties of MgH_2 and MgH_2-BCC Composite. *Int. J. Hydrogen Energy* **2010**, *35*, 7821−7826.

(13) Castro, F. J.; Fuster, V.; Urretavizcaya, G. Hydrogen Sorption Properties of a MgH_2-10wt.% Graphite Mixture. *J. Alloys Compd.* **2011**, *509S*, S595−S598.

(14) Pandyan, R. K.; Seenithurai, S.; Mahendran, M. Hydrogen Storage in MgH_2 Coated Single Walled Carbon Nanotubes. *Int. J. Hydrogen Energy* **2011**, *36*, 3007−3015.

(15) Polanski, M.; Bystrzycki, J.; Varin, R. A.; Plocinski, T.; Pisarek, M. The Effect of Chromium (III) Oxide (Cr_2O_3) Nanopowder on the Microsturcture and Cyclic Hydrogen Storage Behavior of Magnesium Hydride (MgH_2). *J. Alloys Compd.* **2011**, *509*, 2386−2391.

(16) Milošević, S.; Rašković-Lovre, Ž.; Kurko, S.; Vujasin, R.; Cvjetićanin, N.; Matović, L.; Novaković, J. G. Influence of VO_2 Nanostructured Ceramics on Hydrogen Desorption Properties From Magnesium Hydride. *Ceram. Int.* **2013**, *39*, 51−56.

(17) Gupta, R.; Agresti, F.; Russo, S. L.; Maddalena, A.; Palade, P.; Principi, G. Structure and Hydrogen Storage Properties of MgH_2 Catalyzed with La_2O_3. *J. Alloys Compd.* **2008**, *450*, 310−313.

(18) Gulicovski, J.; Rašković-Lovre, Ž.; Kurko, S.; Vujasin, R.; Jovanović, Z.; Matović, L.; Novaković, J. G. Influence of Vacant CeO_2 Nanostructured Ceramics on MgH_2 Hydrogen Desorption Properties. *Ceram. Int.* **2012**, *38*, 1181−1186.

(19) Malka, I. E.; Pisarek, M.; Czujko, T.; Bystrzycki, J. A Study of the ZrF_4, NbF_5, TaF_5, and $TiCl_3$ Influences on the MgH_2 Sorption Properties. *Int. J. Hydrogen Energy* **2011**, *36*, 12909−12917.

(20) Luo, Y.; Wang, P.; Ma, L. P.; Cheng, H. M. Hydrogen Sorption Kinetics of MgH_2 Catalyzed with NbF_5. *J. Alloys Compd.* **2008**, *453*, 138−142.

(21) da Conceicão, M. O. T.; Brum, M. C.; Guimarães, C. S.; dos Santos, D. S. Synthesis and Characterization of Mesoporous PdPtCr Alloy and Its Influence on the Hydrogen Kinetics in MgH_2. *J. Alloys Compd.* **2012**, *536S*, S255−S258.

(22) Mahmoudi, N.; Kaflou, A.; Simchi, A. Hydrogen Desorption Propeprties of MgH_2-$TiCr_{1.2}Fe_{0.6}$ Nanocomposite Prepared by High-Energy Mechanical Alloying. *J. Power Sources* **2011**, *196*, 4604−4608.

(23) Shao, H.; Federhoff, M.; Schüth, F. Hydrogen Storage Properties of Nanostructured MgH_2/TiH_2 Composite Prepared by Ball Milling under High Hydrogen Pressure. *Int. J. Hydrogen Energy* **2011**, *36*, 10828−10833.

(24) Zhang, Y.; Tian, Q. F.; Liu, S. S.; Sun, L. X. The Destabilization Mechanism and De/re-hydrogenation Kinetics of MgH_2-$LiAlH_4$ Hydrogen Storage System. *J. Power Sources* **2008**, *185*, 1514−1518.

(25) Chen, R.; Wang, X. H.; Xu, L.; Chen, L. X.; Li, S. Q.; Chen, C. P. An Investigation on the Reaction Mechanism of $LiAlH_4$-MgH_2 Hydrogen Storage System. *Mater. Chem. Phys.* **2010**, *124*, 83−87.

(26) Vittetoe, A. W.; Niemann, M. U.; Srinivasan, S. S.; McGrath, K.; Kumar, A.; Goswami, D. Y.; Stefanakos, E. K.; Thomas, S. Destabilization of $LiAlH_4$ by Nanocrystalline MgH_2. *Int. J. Hydrogen Energy* **2009**, *34*, 2333−2339.

(27) Milanović, I.; Milošević, S.; Matović, L.; Vujasin, R.; Novaković, N.; Checchetto, R.; Novaković, J. G. Hydrogen Desorption Properties of MgH_2/$LiAlH_4$ Composites. *Int. J. Hydrogen Energy* **2013**, *38*, 12152−12158.

(28) Zheng, X. P.; Xiao, G.; Ma, Q. H.; Liu, S. L.; Li, T.; Feng, X.; Zheng, J. J. Hydrogen Release Capacity of the $LiAlH_4$-MgH_2 System. *J. Power Sources* **2013**, *231*, 173−176.

(29) Ding, X. Q.; Zhu, Y. F.; Wei, L. J.; Li, Y.; Li, L. Q. Synergistic Hydrogen Desorption of HCS MgH_2+$LiAlH_4$ Composite. *Energy* **2013**, *55*, 933−938.

(30) Li, P.; Wan, Q.; Li, Z. L.; Zhai, F. Q.; Li, Y. L.; Cui, L. Q.; Qu, X. H.; Volinsky, A. A. MgH_2 Dehydrogenation Properties Improved by $MnFe_2O_4$ Nanoparticles. *J. Power Sources* **2013**, *239*, 201−206.

(31) Zhai, F. Q.; Li, P.; Sun, A. Z.; Wu, S.; Wan, Q.; Zhang, W. N.; Li, Y. L.; Cui, L. Q.; Qu, X. H. Significantly Improved Dehydrogen-

ation of $LiAlH_4$ Destabilized by $MnFe_2O_4$ Nanoparticles. *J. Phys. Chem. C* **2012**, *116*, 11939−11945.
(32) Wan, Q.; Li, P.; Li, Z. L.; Zhao, K. F.; Liu, Z. W.; Wang, L.; Zhai, F. Q.; Qu, X. H.; Volinsky, A. A. $NaAlH_4$ Dehydrogenation Properties Enhanced by $MnFe_2O_4$ Nanoparticles. *J. Power Sources* **2014**, *248*, 388−395.
(33) Ahmad, M.; Rafi, U. D.; Pan, C. F.; Zhu, J. Investigation of Storage Capabilities of ZnO-based Nanostructures. *J. Phys. Chem. C* **2010**, *114*, 2560−2565.
(34) Li, Z. L.; Li, P.; Wan, Q.; Zhai, F. Q.; Liu, Z. W.; Zhao, K. F.; Wang, L.; Lü, S. Y.; Zou, L.; Qu, X. H.; et al. Dehydrogenation Improvement of $LiAlH_4$ Catalyzed by Fe_2O_3 and Cr_2O_3 Nanoparticles. *J. Phys. Chem. C* **2013**, *117*, 18343−18352.
(35) Mao, J. F.; Guo, Z. P.; Yu, X. B.; Ismail, M.; Liu, H. K. Enhanced Hydrogen Storage Performance of $LiAlH_4$-MgH_2-TiF_3 Composite. *Int. J. Hydrogen Energy* **2011**, *36*, 5369−5374.
(36) Rafi, U. D.; Zhang, L.; Li, P.; Qu, X. H. Catalytic Effects of Nano-sized TiC Additions on the Hydrogen Storage Properties of $LiAlH_4$. *J. Alloys Compd.* **2010**, *508*, 119−128.
(37) Liu, S. S.; Sun, L. X.; Zhang, Y.; Zhang, J.; Chu, H. L.; Fan, M. Qi.; Zhang, T.; Song, X. Y.; Grolier, J. P. Effect of Ball Milling Time on the Hydrogen Storage Properties of TiF_3-doped $LiAlH_4$. *Int. J. Hydrogen Energy* **2009**, *34*, 8079−8085.
(38) Ismail, M.; Zhao, Y.; Yu, X. B.; Dou, S. X. Effects of NbF_5 Addition on the Hydrogen Storage Properties of $LiAlH_4$. *Int. J. Hydrogen Energy* **2010**, *35*, 2361−2367.
(39) Ismail, M.; Zhao, Y.; Yu, X. B.; Nevirkovets, I. P.; Dou, S. X. Significantly Improved Dehydrogenation of $LiAlH_4$ Catalyzed with TiO_2 Nanopowder. *Int. J. Hydrogen Energy* **2011**, *36*, 8427−8334.
(40) Varin, R. A.; Zbroniec, L.; Czujko, T.; Wronski, Z. S. The Effects of Nanonickel Additive on the Decomposition of Complex Metal Hydride $LiAlH_4$ (lithium Alanate). *Int. J. Hydrogen Energy* **2011**, *36*, 1167−1176.
(41) Li, Z. B.; Liu, S. S.; Si, X. L.; Zhang, J.; Jiao, C. L.; Wang, S.; Liu, S.; Zou, Y. J.; Sun, L. X.; Xu, F. Significantly Improved Dehydrogenation of $LiAlH_4$ Destabilized by K_2TiF_6. *Int. J. Hydrogen Energy* **2012**, *37*, 3261−3267.
(42) Ismail, M.; Zhao, Y.; Yu, X. B.; Ranjbar, A.; Dou, S. X. Improved Hydrogen Desorption in Lithium Alanate by Addition of SWCNT-metallic Catalyst Composite. *Int. J. Hydrogen Energy* **2011**, *36*, 3593−3599.
(43) Ismail, M.; Zhao, Y.; Yu, X. B.; Dou, S. X. Effect of Different Additives on the Hydrogen Storage Properties of the MgH_2-$LiAlH_4$ Destabilized System. *RSC Adv.* **2011**, *1*, 408−414.
(44) Kissinger, H. E. Reaction Kinetics in Differential Thermal Analysis. *Anal. Chem.* **1957**, *29*, 1702−1706.